JOURNAL OF RENEWABLE ENERGY AND SMART GRID TECHNOLOGY

Vol. 19, No. 2, July-December 2024

Development of a Long-Range IoT Air Quality Monitoring System Using LoRa Mesh Repeaters for Real-Time Pollution Tracking

Jarun Khonrang[1], Mingkwan Somphruek[1*], Thanapon Saengsuwan[1], Pairoj Duangnakhorn[1] and Atikhom Siri[2]

[1]Faculty of Industrial Technology, Chiang Rai Rajabhat University, Thailand, 57100 Chiang Rai, Thailand
[2]Faculty of Digital Technology, Chiang Rai Rajabhat University, Thailand, 57100 Chiang Rai, Thailand
***Corresponding author's email:** mingkwan.som@crru.ac.th

Article info:

Received: 31 October 2024
Revised: 27 November 2024
Accepted: 28 November 2024
DOI:
10.69650/rast.2024.259538

Keywords:

LoRa Mesh Network
Wireless Internet of Things - Technology (WIoT)
Air Quality Monitoring
Carbon dioxide
PM 2.5

ABSTRACT

Numerous researchers are currently presenting innovative methods to measure air quality in a cost-effective and real-time manner. The primary significance of the air quality monitoring system lies in its ability to facilitate communication via the Internet. This capability enables monitoring stations to measure air quality over extensive regions, spanning several kilometers. Presently, existing technology has constraints on transmitting data beyond distances of a few kilometers. This study introduces an air quality monitoring station capable of measuring NO_2, SO_2, CO_2, CO, PM2.5, and PM10. To extend the transmission range, a LoRa mesh repeater was designed, utilizing point-to-point LoRa technology for extended data transmission. The signal strength between the air quality monitoring station and the repeater varies from -84 dBm to -92 dBm. The observed RSSI signal between the LoRa repeater and the LoRa gateway in the experimental results varies from -69 dBm to -112 dBm. The practical, effective operating distance is 1.7 km, making it suitable for potential utilization in long-distance IoT applications.

1. Introduction

There are many causes of death involved with the level of air quality, as claimed in several studies, such as respiratory or coronary disease causing untimely death in particularly the disabled and the elderly; [1] children's and elderly's health as verified by the survey results; and the increase in deaths from heart disease, asthma, cancer, and Alzheimer's disease at 3.2 million per year due to the dense air pollution [2]. This incidence appeared in both developed and developing countries. From the research data in April 2022, the PM 2.5 in the air in Thailand was higher than the yearly air quality of the WHO four times in 2016, which meant that Thai people inhaled toxic air, which resulted in their health being affected, leading to the deaths of more than 33,000 people [3]. Moreover, Kasetsart University research revealed that the estimated social cost caused by PM 2.5 across the country in 2019 was 2.17 trillion baht per year, which is 11% of the gross product of that year [4]. In 2022, the Department of the European Environmental Agency reported that air pollution was the cause of the deaths of children in Europe aged less than 18 years around 1,200 cases per year and increased the risk of having the ailment of chronic disease [5].

In 2012, the facility industry in the European Union spent around 59–189 billion euros on the release of air pollution. For people, the elderly and children were affected by the air pollution, although they were contacted for a short duration, particularly asthmatic and coronary patients [6]. However, the level of air pollution indoors may be higher than outdoors. That is why indoor air quality (IAQ) was rated one of five environmental risks resulting in world health [7-8]. Thus, IAQ is essential for the well-being of the residents. In general, the elderly and the disabled spend most of their time indoors, which has high significance for many dwellers. From the reports about the IAQ, they indicated that the daily heat-making process and existing needs, such as cooking, depend on burning fuel (coal, charcoal, manure, and husk), which increased significantly [9]. The statistics showed that populations over 4.3 million died untimely due to indoor air pollution, which mainly occurred in moderate and low-income countries in 2012. In conclusion, air quality is a very important issue, mainly in terms of public health [9]. This is done by monitoring the air quality parameters in indoor buildings, which is quite a difficult task for both developing and developed countries. Monitoring air quality is necessary to obtain real-time data and increase awareness of environmental issues. This information can facilitate problem-solving and enable appropriate weather control measures. In the past, data collection involved manual methods, where individuals would physically measure the desired area. The data cannot be displayed continuously due to the problem.

Consequently, the development of an air quality measurement station, a data logger data collection system, and a wireless communication application were undertaken. The issue of communication distance presents a significant challenge to the data collection system. The transmission of data over short distances is limited. Wi-Fi technology has a transmission range of less than 45 m, whereas Bluetooth technology has a transmission range of 100 m [10-11]. IoT technologies such as LoRa and NB-IoT can address transmission distance limitations by enabling data transmission over distances of up to 2 km. However, for longer distances, the received signal may suffer from low signal levels or signal dropouts. One possible solution to address these issues is to enhance the transmission power of the data. In compliance with the IoT standard transmission power regulations in ETSI [12] the maximum allowed power is limited to 25 mW.

This research aims to develop an efficient data transmission system tailored for air quality monitoring stations by enhancing the design of LoRa IoT repeater devices. The objective is to extend the communication range between monitoring stations and the LoRa IoT gateway, thereby achieving broader coverage.

The LoRa repeater receives data from an air quality measuring station operating at 923.2 MHz and forwards the signal to the LoRa gateway operating at 923.4 MHz to avoid inter-channel interference and data collisions, as shown in Fig 1.

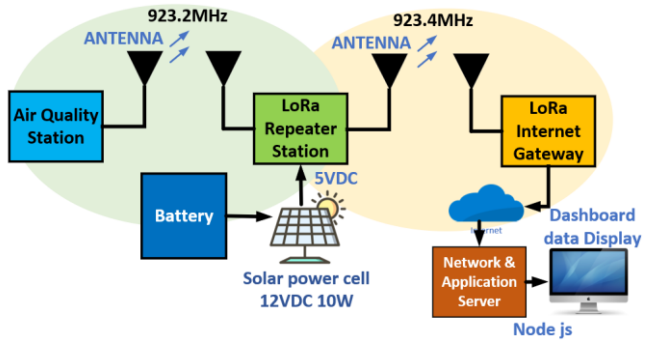

Fig.1 Functional diagram of a repeater system LoRa.

2. LoRa Internet of Things overview

The Internet of Things (IoT) comprises interconnected physical devices that exchange data among themselves. The Internet of Things (IoT) facilitates continuous internet connectivity. This has the potential to enhance machine communication efficiency and reduce power consumption [13-14]. LP-WAN technology was subsequently developed in response to the requirements of machine-to-machine (M2M) communication, which necessitates low power consumption. LP-WAN offers a larger coverage area and reduced expenses compared to cellular networks. LPWAN systems offer several advantages, including low data transfer speeds and minimal energy consumption from connected devices. LPWAN technology offers various options in IoT and M2M communication, catering to specific requirements and utilities such as data speed, budget, frequency, network cost, size capacity, and safety [13]. However, LPWAN technology can be widely divided into two types: licensed LPWAN technologies such as NB-IoT, LTE-M-IoT, EC-GSM-IoT, and 5G IoT, and non-licensed LPWAN technologies such as SigFox, Telensa, LoRa, and RPMA. However, this research focuses mainly on LoRa technology (Long Range), a wireless digital internet of things (IoT) that can transmit data over distance of more than 10 km in rural areas. LoRa technology finds applications in various industries such as mining, natural resource management, alternative power, and long-distance transportation. LoRa technology can be categorized into three classes [15].

Class A: This technology uses low power and general equipment and is divided into 2 types: sending uplink signals set up by terminal equipment as needed using the ALOHA protocol and sending downlink signals consisting of 1 channel followed by 2 downlink channels. Class A is terminal equipment for LoRa with a low electrical system.

Class B: The signal-receiving window is applied more at the time of downlink communication, having the delay time as a setting, but the additional power is used in the terminal equipment. Besides, the additional power, which is low enough to use the application, consumes power from the battery.

Class C: It functions by reducing the time spent transmitting the downlink signal by turning on the equipment every time it sends the signal. Class C uses more power and has the lowest delay compared with classes A and B.

This study utilizes the Internet of Things and LPWAN LoRa, a communication system, to monitor and assess air quality. The objective of this study is to enhance public awareness regarding health, safety, convenience, and air quality. And focuses on a real-time air quality monitoring station that utilizes both wireless sensors and a network to gather air quality data. Moreover, this technology can be implemented in a sustainable manner through the utilization of solar energy to charge a battery, which can then be connected to an external electrical power distribution system. The system offers several advantages, including accessibility, cost-effectiveness, long-range capability, extensive coverage, self-power distribution, extended battery life, immediate responsiveness, and scientific validation of its accuracy.

3. Hardware design and installation

3.1 LoRa air quality sensor node

This work introduces a real-time air quality monitoring station that utilizes the Internet of Things (IoT) technology. The station employs LoRa to transmit data on the gas intensity of PM, enabling low-energy consumption and long-distance data transmission. The collected data is then analyzed and presented to the user. The Arduino Mega 2560 is utilized as the sensor node in this study. The detection module is comprised of gas and particulate matter (PM) sensors, specifically NO_2, SO_2, CO, PM10, and PM2.5 sensors, which are connected to the sensors. The system includes the MQ-9 module, MG-811 carbon monoxide sensor, MQ-131 carbon dioxide sensor, 2SH12 nitrogen dioxide sensor, sulfur dioxide sensor, and PMS3003, PM2.5, and PM10 particulate matter sensors. Fig. 2 illustrates the linkage between the sensors and the microcontroller. This connection is established through a 12-bit analogue input, which facilitates the integration of the airborne dust sensor via the USART communication channel. The module utilizes SPI serial communication to interface with LoRa technology, specifically the SX1276 chip.

3.2 Multi-sensor

The environmental monitoring tool comprises an array of sensors that measure parameter values in various air conditions. The selection of the sensor is based on its key characteristics, including

accuracy and low power consumption. The sensor's characteristics, specifically its sensitivity to the target gas, are summarized in Table 1.

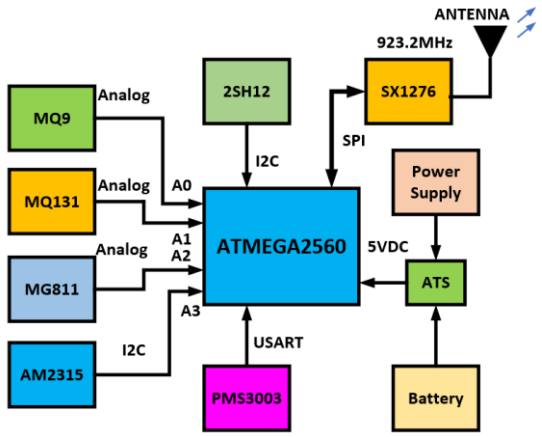

Fig. 2 Diagram of an air quality node sensor for research purposes.

In terms of electrochemical CO, SO_2, CO_2, and NO_2 sensors, the sensor was applied by separating each electrode, differing from designs that integrate multiple electrodes into a single sensor. While sensors with multiple electrodes are capable of measuring various types of gases, they have the disadvantage of lower accuracy compared to sensors with separated electrodes. In measuring the value of the dust in the air, the air dust monitoring laser utilizing scattering laser technology was employed to measure PM10 and PM2.5.

Table 1 The characteristics of the sensors.

GAS SENSORS				
Sensor	Target Gas	Range (ppm)	Resolution (ppm)	Response Time (s)
MQ-9	CO	100 - 10000	10 - 1000	<60
MG-811	CO_2	350 - 10,000	10 - 1000	<60
MQ-131	NO_2	10-1000	10ppb - 2	<100
2SH12	SO_2	1-500	1 - 500	≤30
AM2315C	Temp & Humidity	-20 - 80°C 0-100% Humidity		
Particulate Matter				
Sensor	sensor type	Range (μm)	Resolution (μg/m³)	Response Time (s)
PMS3003 Laser Dust Sensor	PM2.5	0 - 500	1	<10
	PM10	0 - 500	1	<10

3.3 LoRa repeater

In the design of a LoRa repeater, the incorporation of renewable energy sources is essential due to the remote installation locations where access to conventional power sources is limited. Solar cells are commonly utilized in conjunction with a backup battery to ensure uninterrupted operation of the system. LoRa technology's low power consumption makes it well-suited for utilization with alternative energy sources. Fig. 3 illustrates the connection diagram for a LoRa repeater. The system consists of an Arduino Nano microcontroller that is connected to two LoRa SX1276 modules through serial peripheral interface (SPI) and a microcontroller. Both modules operate in distinct frequency bands. While the sensor node communicates on the 923.2 MHz frequency band, the LoRa gateway communicates on the 923.4 MHz frequency band. Table 2 displays the parameters of the LoRa communication system.

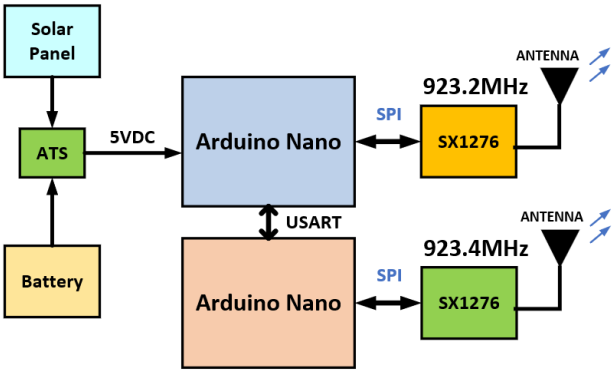

Fig. 3 Connection diagram of the LoRa repeater.

Table 2 The parameters on figuration of the LoRa.

Parameters	Configuration
Bandwidth(BW)	125 kHz
Node transmitting power	20 dBm
Repeater transmitting power	20 dBm
Node spreading factor (SF)	7
Repeater spreading factor (SF)	7
Node to Repeater Frequency Channel	923.2 MHz
Repeater to Gateway Frequency Channel	923.4 MHz
Antenna gain	3 dBi
Transmit time interval	1 s
Node to repeater Tx/Rx height	1.7 m
Repeater to gateway to repeater Tx/Rx height	1.7 m

4. The LoRa point-to-point communication measurement setup and procedure

In this section, the design of point-to-point communication for LoRa IoT is focused on, with LoRa's unique characteristics integrated to establish a robust data communication system. The design process includes the calculation of path loss in the transmission system, as well as measurements and testing conducted to ensure that the LoRa IoT network provides adequate area coverage. The goal is to validate that the design aligns with both theoretical calculations and experimental results.

LoRa employs spread-spectrum modulation, specifically chirp spread spectrum (CSS), to achieve connectivity, modulating symbols over a fixed bandwidth using chirps. The spreading factor (SF) governs the number of chirps per symbol, with higher SF values extending range but reducing data rate and increasing transmission duration, which subsequently raises energy consumption [16]. Each SF offers distinct advantages, as shown in Table 3. The LoRa modulation technique thus enables a trade-off between range and energy efficiency by adjusting the SF according to the received signal strength indicator (RSSI) and signal-to-noise ratio (SNR), impacting both transmission distance and bandwidth. This study considers these aspects in the design, selecting optimal SF values to maximize coverage and maintain efficiency.

Table 3 LoRa demodulator (bw125 kHz) sensitivity for RSSI and SNR.

Spreading factor	RSSI (dBm)	SNR (dB)
SF6	-118	-5
SF7	-123	-7.5
SF8	-126	-10
SF9	-129	-12.5
SF10	-132	-15
SF11	-133	-17.5
SF12	-136	-20

Fig. 4 The installation location of the LoRa node air quality station.

To ensure effortless installation of peer-to-peer (P2P) links. By mounting the node to the wall of the air quality monitoring station, as depicted in Fig. 4. A height of 1.7 m was assumed for convenience. The expansion of LoRa point-to-point links into a mesh network is expected to provide comparable benefits in terms of deployment convenience and flexibility. A platform based on a LoRa modem has been developed, with both the hardware, including an SX1276, and the software being open-source to enhance reproducibility [17-19]. A significant difference between the two groups was observed in the experiment.

It has developed an experimental setup consisting of short antennas and receivers. This setup is designed to mimic scenarios where simple antenna and gateway setups are needed. The objective of the point-to-point communication experiment is to determine the maximum transmission range of the LoRa module. The LoRa air quality sensor node will be permanently installed at the specified location of the measuring station. The LoRa test node is relocated from the LoRa air quality sensor node to assess the received signal strength indicator (RSSI) and the maximum transmission distance.

The path loss calculation estimates the potential loss and the minimum received signal level for a given distance. The equipment installation site for line-of-sight calculations is an open area influenced by environmental factors. The path loss models are used to predict the decrease in signal power as it travels through a medium. These effects encompass the expansion of radio waves as well as phenomena such as reflection, scattering, diffraction, and absorption. The environment affects the path loss, the distances between the transmitter and receiver, and the heights of the transmit and receive antennas. The parameters of the path loss model are generally applicable only within specific frequency ranges, antenna configurations, and environmental conditions. The conventional model for path loss (PL) is a log power law with a random component [20-21]. Equation (1) represents the log-distance path loss model in decibels (dB).

$$path_{loss_m}(d) = PL(d_0) + 10nlog_{10}\left(\frac{d}{d_0}\right) + X\sigma, d \geq d_0 \quad (1)$$

Where n is the path loss exponent, d represents the distance, measured in meters, between the receiver and transmitter. The term $X\sigma$ refers to the variability observed around the average value. Additionally, $N(0,\sigma^2)$ is a model used to represent large-scale fading. While $PL(d_0)$ is the path loss at a reference distance of d_0. A reference distance d_0 of 1 m was used for the modelling experiments. Meanwhile, the estimation of $PL(d_0)$ is obtained through the fitting method applied to the measured data. The subscript m represents the modelled path loss, while s represents the sampled path loss. Additionally, the standard deviation σ can be conceptualized as either a constant scalar or a variable that depends on distance, which can be obtained from Equation (2).

$$\sigma(d) = alog_{10}\left(\frac{d}{d_0}\right) + b \quad (2)$$

The present investigation utilizes the wireless data-sending module LoRa SX1276, which operates at a transmission strength of 20 dBm throughout the frequency range of 923.2 MHz and 923.4 MHz. However, the path loss is primarily determined by the wide angle at which the wave is emitted. This causes the dense wave signal to gradually weaken as the distance increases due to the spreading of the wave in free space propagation, as represented by Equation (3).

$$\frac{P_R}{P_T} = G_T G_R \left[\frac{\lambda}{4\pi d}\right]^2 \quad (3)$$

P_R is measuring the signal power unit in (dBm).

P_T is the transmitted power in decibels (dBm).

G_R refers to the unit of receiver an antenna expansion (dBi).

G_T is an expanded rate of the sender an antenna unit (dBi).

λ is the wavelength value, which $\lambda = c/f$.

C is light speed $(3 \times 10^8 m/s)$.

f is the signal frequency unit (Hz).

d represents the distance, measured in meters, between the receiving and sending sections.

Therefore, the signal power loss in the air is quantified in decibels (dB) using Equation (4).

$$L_{dB} = 10\,log(P_T) - 10\,log(P_R) \quad (4)$$

When selecting an antenna for transmitting and receiving signals, it is important to use the same type of antenna, specifically a monopole antenna with power expansion capability and a size of 3 dBi. The given values are P_T = 20 dBm and G_R and G_T = 3 dBi, with a wavelength (λ) of 0.324 m and 1 km between the receiver and transmitter.

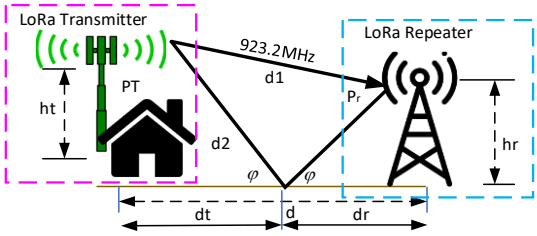

Fig. 5 The calculation diagram and the design of the data-sending system.

Fig. 5 illustrates the distinct paths and varying distances travelled by both signals. Consequently, upon reaching the receiving antenna, the signals may exhibit a phase shift. Therefore, it is necessary to include a calculation for the disparity in the distance of the two waves in Equation (5).

$$\Delta d = d_2 - d_1 = \sqrt{(h_t - h_r)^2 + {d_2}^2} - \sqrt{(h_t - h_r)^2 + {d_1}^2} \quad (5)$$

The $RSSI$ value is subject to change based on the strength of the signal. A high signal strength value indicates proximity between the receiver and transmitter, while a low signal strength value indicates distance between them [22]. The calculation can be performed using Equation (6).

$$RSSI = -10n\, log_{10}\, d + A \quad (6)$$

where n is the loss exponent in the path, usually given n = 2, d is the distance between the transmitter and the receiver, and A = 1 represents the received power in dBm when the distance between the antennas. The signal-to-noise ratio of the transmitter and receiver is measured in meters, where the $RSSI$ value is measured in dBm, and the signal-to-noise ratio can be obtained from Equation (7) [23].

$$SNR = 174 + RSSI - P_{tx} - 10\, log_{10}\, BW - NF \quad (7)$$

P_{tx} represent the transmission power of the transmitter, BW denotes the amplitude of the transmitting frequency in kHz, NF indicates the noise value of the transmitter and receiver, and 174 represent the thermal noise, which has a bandwidth of 1 Hz and is solely dependent on the temperature of the receiver.

As depicted in Fig. 6, As depicted in Fig. 6, the air quality monitoring station was installed in a real location within Dongmada Sub-district Municipality, Mae Lao District, Chiang Rai Province, for system testing. A stationary setup was established on the TX side, consisting of a single transceiver programmed to transmit packets at SF7.

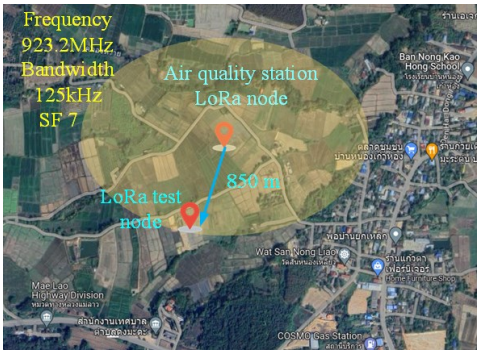

Fig. 6 The map and the distance between the air quality monitoring station and the LoRa test node.

Fig. 6 illustrates the map and the distance between the air quality monitoring station and the LoRa test node installed at Dongmada Sub-district Municipality in Chiangrai Province, Thailand, which has a long distance of 850 m. When measuring the RSSI value of the received signal 10 times, the strength of the received signal is around -89 dBm.

Fig. 7 shows the LoRa test node board to measure the signal strength that the air quality station LoRa node transmits. The ATMEGA2560 microcontroller is linked to the LoRa module SX1276. However, at 850 m in the experiment, the signal level measured -89 dBm. The value does not represent the maximum communication distance. However, it is important to consider factors that can lead to signal attenuation, such as rainy weather, in practical scenarios. Despite this, the communication system will still function effectively at this distance. Therefore, the LoRa repeater will be installed at a point 850 m away, which is half the distance between the air quality station LoRa node and the LoRa gateway.

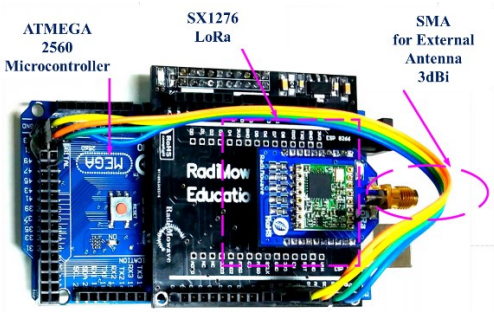

Fig. 7 LoRa nodes for testing signal strength and distance.

5. The LoRa mesh communication measurement setup

Monitoring systems for linear utilities, such as power lines, waterways, and piping systems, are frequently employed in Internet of Things (IoT) implementations. Although LoRa offers extended transmission ranges, it may not be suitable for utility systems that span over ten kilometers and require the deployment of gateways at regular intervals. Underground deployments in sewage systems, mines, and other similar environments also face coverage challenges. For example, Duong et al. developed and executed a multi-hop communication protocol for LoRa networks that can cover extensive distances [24-25]. The proposed solution is designed for deployments in which monitoring nodes are positioned linearly, such as along a gas pipe or high-voltage line. Devices synchronize and awaken at predetermined intervals to receive data packets from neighboring devices. They can then merge these packets with their own and transmit them to subsequent devices in the network. Downlink data transmission is not addressed.

Additionally, Abrardo et al. developed a multi-hop LoRa linear network for underground environments, focusing on optimizing the sleep and wake cycles of nodes to minimize battery usage [26]. The researchers discovered that LoRa transmission had a range limitation of approximately 200 m. As a result, the star topology was deemed unsuitable for effectively monitoring lengthy aqueducts with obstructed lines of sight due to curves. To deal with this constraint, the researchers chose to implement a data propagation model using sensor nodes that form a transmission chain leading to the gateway. They also incorporated a synchronization mechanism to optimize the duration of sleep cycles when transmitting data between pairs of nodes.

To overcome the limitations of using LoRa distance in a star-to-star topology, LoRa has been implemented in the form of a mesh network. This allows for increased transmission distance within the system. However, after successfully designing and testing point-to-point data transmission with an SF value of 7 and a transmission distance of 850 m, the average RSSI value is approximately -89 dBm. Based on the experimental findings, the selected value of SF 7 is relatively low. SF 7 is capable of transmitting data over a certain distance; it can be inferred that higher SF values will also transmit data. LoRa enables longer signal reception as the value of the spreading factor (SF) increases. For instance, a higher spreading factor (SF) such as SF 10 enables the transmission of data over a greater distance compared to a lower spreading factor like SF 8. Increasing the value of SF will result in a decrease in data transmission bandwidth.

Fig. 8 The installation location of the LoRa repeater.

In the experimental implementation of LoRa mesh with a LoRa repeater, various transmission frequency bands were utilized. Hence, the issue of cross-channel interference can be resolved. Data collisions occur when two or more devices attempt to transmit data simultaneously on a shared network, resulting in a disruption or loss of data. A LoRa repeater is designed by utilizing two LoRa modules to establish a connection between them. The communication between two ATMEGA328 microcontrollers (specifically the Arduino nano) is facilitated through a serial port, as depicted in Fig. 3. Additionally, Fig. 8 illustrates the hardware and installation of the LoRa repeater in operation.

In the experimental phase of transmitting data from the air quality LoRa station to the gateway, three different spreading factors (SF) values will be employed: SF 7, SF 9, and SF 10. This approach aims to compare the packet delivery ratio (PDR) and delivery time. The experiment aims to assess the impact of the distance between the LoRa repeater and the LoRa gateway on the measurements of PDR (packet delivery ratio) and delivery time. The experiment observed the movement of a LoRa gateway connected to a cellular internet signal, which varied in distance from a LoRa repeater between 300 m and 1,000 m. Fig. 9 depicts the LoRa gateway device utilized in the experiment. The LoRa modules were tested by transmitting data at a fixed output power level of 20 dBm and a bandwidth of 125 kHz over varying distances.

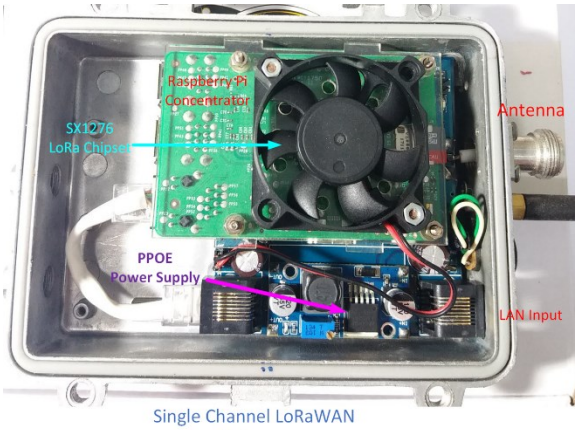

Fig. 9 The single channel LoRa gateway device.

There are two nodes in the system: an air quality station node and a repeater node. Both nodes are located at a height of 1.7 m above ground. Position the receiver in the same unobstructed plane as the transmitter. This experiment assessed the packet delivery ratio (PDR) of nodes configured with different spreading factors (SF) settings, specifically SF values of 7, 9, and 10. The results of the experiment indicate that increasing the value of SF leads to higher values of PDR. Additionally, as the distance increases, the value of PDR decreases in a distance-dependent manner.

Fig. 10 shows that SF = 10 yielded the best PDR among all the tested distances. The PDR was 55% when SF was 7 at 300 m, and the percentage decreased to 18% at 1,000 m. It was observed that the PDR at 400 m was 97% at an SF value of 10, which was significantly better than the PDR at an SF value of 7. This experiment verified that increasing the numerical value of the spreading factor (SF) can enhance both the transmission range and data delivery performance. However, increasing the value of SF results in an increase in PDR, although it also leads to a corresponding increase in latency.

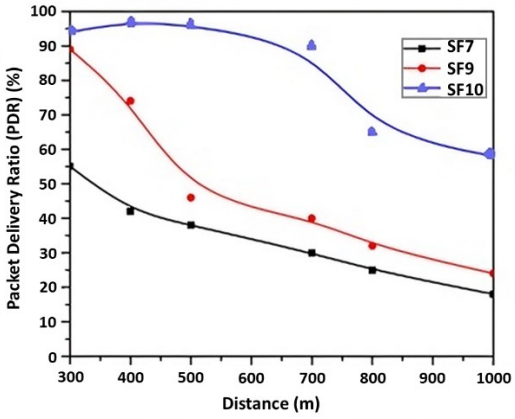

Fig. 10 The values of PDR at different distances under different SF settings.

where the value of the packet delivery ratio, or PDR, can be obtained from the Equation (8) [27].

$$PDR = \frac{P_{success}}{P_{sends}} \quad (8)$$

$P_{success}$ represents the successful transmission of packets, while P_{sends} represents the total number of packets sent and provides network data collected from all sending nodes.

Fig. 11 depicts the installation map of the transmission equipment connecting the air-quality LoRa station, LoRa repeater, and LoRa gateway. The total installation distance is approximately 1.7 km. The LoRa gateway is installed at Dongmada Subdistrict Administrative Organization in Mae Lao District, Chiang Rai Province, Thailand. Fig. 12 depicts the placement of the LoRa gateway and LoRa network server during the installation process.

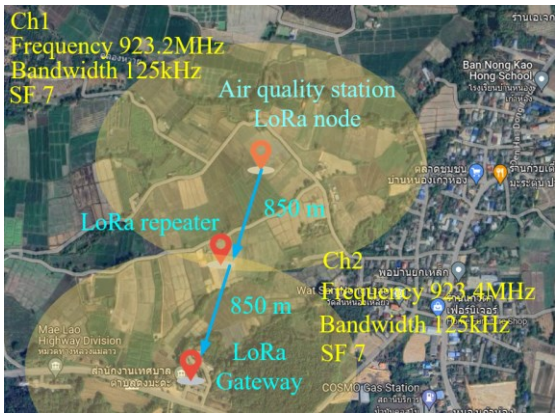

Fig. 11 The transmission distance map from the air quality LoRa station to the LoRa gateway and installation point.

When employing a mesh transmission model, it is crucial to consider the time-on-air value of the packet. This is because the time-on-air value increases with greater distances or a higher number of transmissions.

In the upcoming experiment, the duration of data transmission in a two-hop system comprising an air-quality LoRa node, a LoRa repeater, and a LoRa gateway will be investigated. The bandwidth and spreading factor (SF) of data transmission will be manipulated during the experiment. The experimental results will focus on airtime.

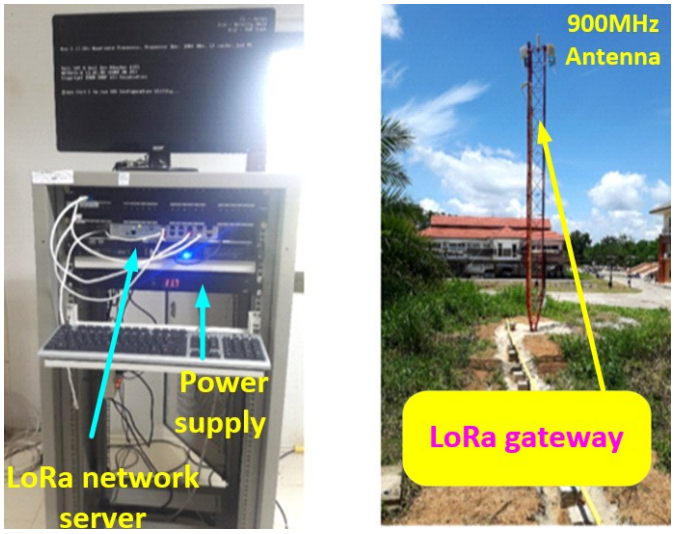

Fig. 12 The LoRa gateway and LoRa network server utilized in this study.

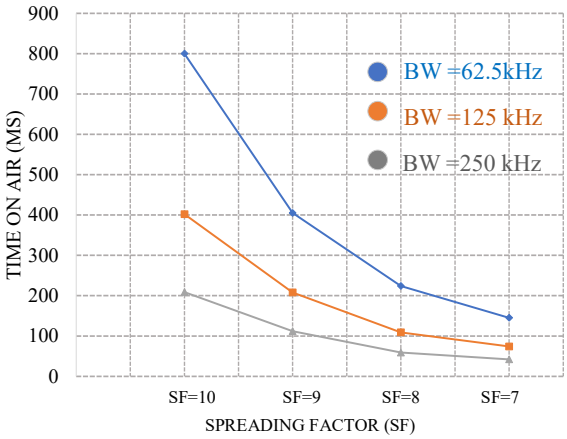

Fig. 13 Time on air under different SF and BW settings.

Fig. 13 demonstrates the impact of various bandwidth (BW) and spreading factor (SF) configurations on the period of wireless data transmission, also known as time on air. The objective is to examine the impact of SF and BW on airtime. It was found that an increased period of airtime was associated with a larger SF and a smaller BW. The airtime period was 42 ms in the case of the spreading factor (SF), which was initially 7 with a bandwidth (BW) of 250 kHz. However, increasing the SF to 10 and reducing the bandwidth to 62.5 kHz resulted in an increase in the time duration to 800 ms.

6. Results and Discussion

The experimental results, presented in Fig. 14, illustrate the data from a daily air quality measurement of carbon dioxide levels. Fig. 15 displays the recorded nitrogen dioxide concentrations obtained from the measurement samples collected over a single day, as indicated by the experimental results. Fig. 16 displays the recorded measurement results of sulfur dioxide gas obtained from a single day's sampling in the experiment. Fig. 17 displays the recorded measurements of PM2.5 and PM10 dust levels obtained from a single day of sampling.

Fig. 18 presents the experimental results of the RSSI signal level between the air quality monitoring station and the LoRa repeater. The signal level observed ranges from -84 dBm to -92 dBm. LoRa can receive signals at a satisfactory level. However, the SX1276 chip number indicates the ability to receive signals at a minimum level of -123 dBm at SF 7.

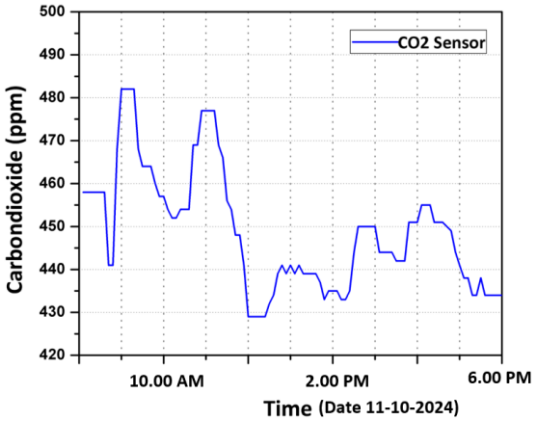

Fig. 14 The recorded carbon dioxide levels.

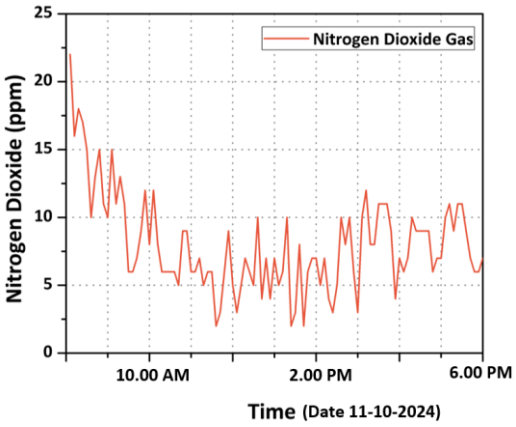

Fig. 15 The measurable levels of nitrogen dioxide.

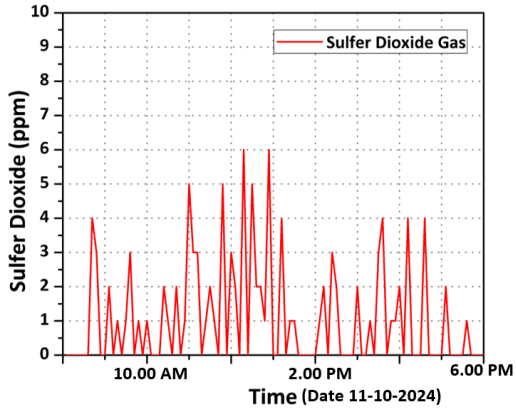

Fig. 16 The recorded levels of sulfur dioxide gas.

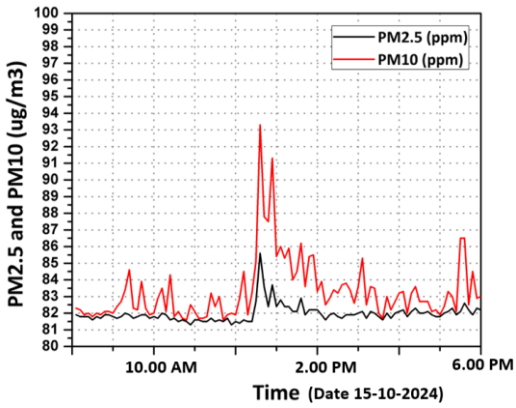

Fig. 17 The levels of particulate matter (PM2.5 and PM10).

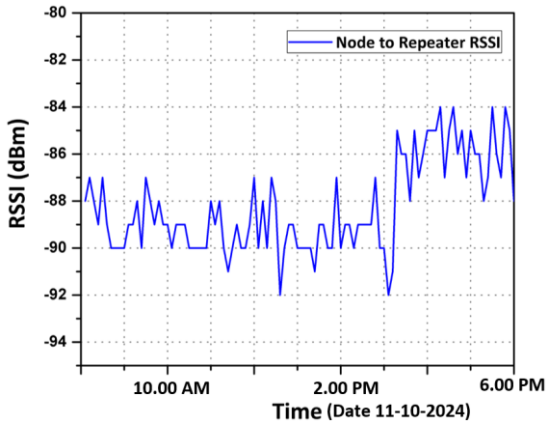

Fig. 18 RSSI level between air quality monitoring station and LoRa repeater.

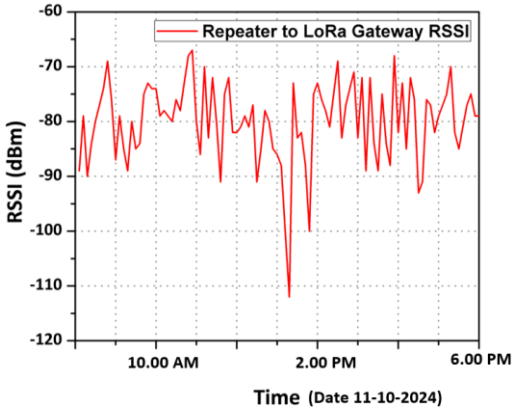

Fig. 19 RSSI level between LoRa repeater and LoRa gateway.

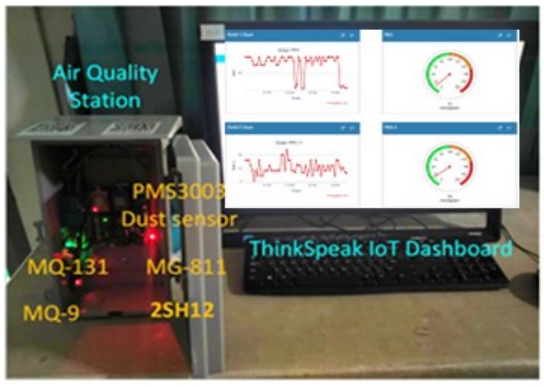

Fig. 20 The prototype air quality monitoring station equipment.

Fig. 19 displays the Received Signal Strength Indicator (RSSI) signal level between the LoRa repeater and the LoRa Gateway. The experimental results indicate that the average signal level ranges from -69 dBm to -112 dBm. At a high level, the strength of the signal is greater compared to a low level.

The ATMEGA2560 microcontroller links to a prototype air quality station device, as illustrated in Fig. 20. Various air quality sensors such as MQ131, MQ9, MG811, 2SH12, and PMS3003 connect to this device. The LoRa gateway receives data from the air quality station and connects to the embedded systems through an SPI interface. The Raspberry Pi Internet IoT serves as a gateway to send data from the internet system to the network and application server. Think speak displays the electrical power values on the dashboard.

7. Conclusion

The research design and implementation suggest that employing repeater techniques in air quality monitoring stations using LoRa technology is effective. The signal level between the air quality monitoring station and the repeater ranges from -84 dBm to -92 dBm. The RSSI signal between the LoRa repeater and the LoRa Gateway, as observed in the experimental results, ranges from -69 dBm to -112 dBm. In practice, the effective operating distance is 850 m. An SF of 7 can be implemented, resulting in a PDR value of 25% frequency. This system has the potential to extend the range of the internet using LoRa technology in various sectors, including industrial and agricultural applications, in the future.

In practical applications, it is important to consider the significance of the packet delivery ratio (PDR) as it pertains to the loss of data during communication, resulting in discretely received data. The analysis of the experimental results shows that using SF 10 with a bandwidth of 125 kHz achieves the highest PDR value of 65%. In practical application, SF 7 is usable; nevertheless, in terms of transmission efficiency, SF 10 is a preferable alternative. However, a potential drawback is the increase in time-on-air value.

Due to the effectiveness of data transmission, weather conditions impact the recommendations for the situation. To enhance transmission power, one can increase the antenna's gain. Both the sender and receiver will enhance the system's efficiency correspondingly.

Acknowledgments

The success of this research was under the support and the assistance from Thailand Science Research and Innovation and Chiang Rai Rajabhat University, Project code FRB 660 028. 0192-14, Budget year 2023.

References

[1] Pope, C. A. III., Burnett, R. T., Thurston, G. D., Thun, M. J., Calle, E. E., Krewski, D. and Godleski, J. J., Cardiovascular mortality and long-term exposure to particulate air pollution: epidemiological evidence of general pathophysiological pathways of disease. *Circulation*. 109(1) (2004) 71-77, doi: http://doi.org/10.1161/01.cir.0000108927.80044.7f.

[2] Dockery, D. W., Pope, C. A. III., Xu, X., Spengler, J. D., Ware, J.H., Fay, M. E., Ferris, B. G. Jr., Speizer and F. E., An association between air pollution and mortality in six U.S. cities. *The New England Journal of Medicine*. 329 (1993) 1753-1759, doi: http://doi.org/10.1056/nejm199312093292401.

[3] World Health Organization (WHO), WHO's global air-quality guidelines. *The Lancet*. 368 (2006) 1302, doi: http://doi.org/10.1016/s0140-6736(06)69530-5.

[4] Witsanu, A. *Final report willingness to pay for air quality in Thailand: An analysis of multiple pollutants: Research paper no. 15/2021,* Kasetsart University, Bangkok (Thailand). Faculty of Economics. Department of Economics, 2021.

[5] European Environment Agency. *Air quality in Europe 2022,* <https://www.eea.europa.eu/publications/air-quality-in-europe-2022> (2022).

[6] European Environment Agency. *Costs of air pollution from European industrial facilities 2008-2012*, <https://www.eea.europa.eu/publications/costs-of-air-pollution-2008-2012> (2014).

[7] EPA United States Environmental Protection Agency, *The Inside Story: A Guide to Indoor Air Quality*, <https://www.epa.gov/indoor-air-quality-iaq/inside-story-guide-indoor-air-quality > (2023).

[8] Rungrat, V., Kamol, B., Elena, M., Tim, A., Nonchanutt, C., Unalome, W. H., Ian, R., Virginia, P., Joachim, O. and Nutapong, S., Electromagnetic Property Characterization and Sensing of Endothelial Cells Growth Medium and Dulbecco's Phosphate Buffered Saline Solution for in vitro Cell Culture in *19th International Conference on Electrical Engineering/Electronics, Computer, Telecommunications and Information Technology, ECTI-CON.* (2022), 1-4, doi: http://doi.org/10.1109/ecti-con54298.2022.9795438.

[9] Tran, V.V., Park, D. and Lee, Y.C., Indoor Air Pollution Related Human Diseases and Recent Trends in the Control and Improvement of Indoor Air Quality. *International Journal of Environmental Research and Public Health*. 17(8) (2020) 1-27, doi: http://doi.org/10.3390/ijerph17082927.

[10] Pradhan, B., Bhattacharyya, S. and Pal, K., IoT-Based Applications in Healthcare Devices. *Journal of Healthcare Engineering*. 2021(1) (2021), doi: http://doi.org/10.1155/2021/6632599.

[11] Kamol, B., Rungrat, V., Robertson, I. D., Tim, A., Chudpooti, N. and Nutapong, S. Illumination and Bandwidth Control Circuit for LED Optical Wireless Transmitter Driver Integrated with Passive Second-Order Equaliser for Pipe Robot Application. in *2023 Research, Invention, and Innovation Congress: Innovative Electricals and Electronics (RI2C)*. (2023), 13-17, doi: http://doi.org/10.1109/ri2c60382.2023.10356036.

[12] Antipolis, S. *ETSI releases first globally applicable standard for consumer IoT security*, <https://www.etsi.org /newsroom/press-releases/1549-2019-02-etsi-releases-first-globally-applicable-standard-for-consumer-iot-security> (2019).

[13] Jarun, K., Minkwan, S., Piroj, D., Atikhom, S. and Kamol, B., Experimental and Case studies of Long distance Multi-hopping Data Transmission Techniques for Wildfire Sensors Using the LoRa-Based Mesh Sensor Network. *International Journal of Electronics and Telecommunications*. 69(3) (2023) 419-424, doi: https://doi.org/10.24425/ijet.2023.144378.

[14] Kamol, B., Pongsathorn, C. Weijia, Z., Timothy, J. A., Joachim, O., Ian, D. R. and Nutapong, S. Advanced Studies on Optical Wireless Communications for in-Pipe Environments: Bandwidth Exploration and Thermal Management. *IEEE Access.* 12 (2024) 80607-80632, doi: http://doi.org/0.1109/access.2024.3410465.

[15] Sinha, R. S., Wei, Y. and Hwang, S. H., A survey on LPWA technology: LoRa and NB-IoT. *ICT Express*. 3 (2017) 14–21, doi: https://doi.org/10.1016/j.icte.2017.03.004.

[16] SEMTECH Corporation. *LoRa and LoRaWAN: Technical overview | Developer Portal*, <https://loradevelopers.semtech.com/documentation/tech-papers-and-guides/lora-and-lorawan/> (2022).

[17] SEMTECH Corporation. *SX1276*, <https://www.semtech.com/products/wireless-rf/lora-connect/sx1276#documentation> (2024).

[18] Kamol, B., Rungrat, V., Panuvat, J., Jessada, K., Nonchanutt, C., Ian, R., Tim, A. and Nutapong, S. Active Pre-Equalizer for Broadband Optical Wireless Communication Integrated with RF Amplifier. in *2022 Research, Invention, and Innovation Congress: Innovative Electricals and Electronics (RI2C),* (2022) 251-254, doi: http://doi.org/10.1109/ri2c56397.2022.9910315.

[19] Kamol, B., Pratumvinit, T. and Akkaraekthalin, P., A compact microstrip two-layers bandpass filter using improved interdigital-loop resonators. in *2009 IEEE International Symposium on Radio-Frequency Integration Technology (RFIT)*. (2009), 367-370.

[20] Africa, A. D. M., Bulda, L. R., Rosario, E. D., Marasigan, M. Z. and Navarro, I., Radio Wave Propagation: Simulation of Free Space Propagation Path Loss. *International Journal of Emerging Trends in Engineering Research*. 8(2) (2020) 281–287. doi: https://doi.org/10.30534/ijeter/2020/07822020.

[21] Kamol, B., Jarun, K., Rungraungsilp, S. and Amsdon, T., Robertson, I., and Nutapong, S., Advancing In-Pipe Robot Communication with High-Speed OWC Transceiver Front-End Circuit: Experimental Insights and Prospects. in *2024 21st International Conference on Electrical Engineering/ Electronics, Computer, Telecommunications and Information Technology (ECTI-CON)*. (2024) 1-6, doi: http://doi.org/ 10.1109/ecti-con60892.2024.10595010.

[22] Shang, F., Su, W., Wang, Q., Gao, H. and Fu, Q. A., Location Estimation Algorithm Based on RSSI Vector Similarity Degree. *International Journal of Distributed Sensor Networks*. 10(8) (2014) 1-22, doi: http://doi.org/10.1155/2014/371350.

[23] The Things Industries. *RSSI and SNR.* <https://www.thethingsnetwork.org/docs/lorawan/rssi-and-snr/> (2024).

[24] Leonardi, L. Lo., Bello, L. and Patti, G., MRT-LoRa: A multi-hop real-time communication protocol for industrial IoT applications over LoRa networks. *Computer Communications*. 199 (2023) 72–86.

[25] Nie, X., Kamol, B, Ma, C., Cheng, L., Roberston, I. D. and Qing, A. An Accurate Imaging Algorithm with Dual-Path Propagation Loss for Monostatic System. in *IEEE International Symposium on Antennas and Propagation and USNC-URSI Radio Science Meeting (USNC-URSI)*. (2023), 471-472.

[26] Abrardo, A. and Pozzebon, A., A Multi-Hop LoRa Linear Sensor Network for the Monitoring of Underground Environments: The Case of the Medieval Aqueducts in Siena, Italy. *Sensors*. 19 (2019) 1-22, doi: https://doi.org/10.3390/s19020402.

[27] Liang, R., Zhao, L. and Wang, P., Performance Evaluations of LoRa Wireless Communication in Building Environments. *Sensors*. 20 (2020) 1-19, doi: http://doi.org/10.3390/s20143828.